Three Modes of Proton Transfer in One Chromophore: Photoinduced Tautomerization in 2-(1 H -Pyrazol-5-yl)Pyridines, Their Dimers and Alcohol Complexes

ARTICLE *in* CHEMPHYSCHEM · NOVEMBER 2012

Impact Factor: 3.42 · DOI: 10.1002/cphc.201200602 · Source: PubMed

8 AUTHORS, INCLUDING:

Volha Vetokhina
Polish Academy of Sciences
10 PUBLICATIONS **39** CITATIONS
SEE PROFILE

Krzysztof Dobek
Adam Mickiewicz University
33 PUBLICATIONS **350** CITATIONS
SEE PROFILE

J. Waluk
Polish Academy of Sciences
257 PUBLICATIONS **3,690** CITATIONS
SEE PROFILE

Jerzy Herbich
Instytut Chemii Fizycznej PAN
46 PUBLICATIONS **1,100** CITATIONS
SEE PROFILE

DOI: 10.1002/cphc.201200602

Three Modes of Proton Transfer in One Chromophore: Photoinduced Tautomerization in 2-(1*H*-Pyrazol-5-yl)Pyridines, Their Dimers and Alcohol Complexes

Volha Vetokhina,[a] Krzysztof Dobek,[b] Michał Kijak,[a] Izabela I. Kamińska,[c] Keven Muller,[d] Werner R. Thiel,[d] Jacek Waluk,[a, c] and Jerzy Herbich*[a, c]

Studies of 2-(1*H*-pyrazol-5-yl)pyridine (PPP) and its derivatives 2-(4-methyl-1*H*-pyrazol-5-yl)pyridine (MPP) and 2-(3-bromo-1*H*-pyrazol-5-yl)pyridine (BPP) by stationary and time-resolved UV/Vis spectroscopic methods, and quantum chemical computations show that this class of compounds provides a rare example of molecules that exhibit three types of photoreactions: 1) excited-state intramolecular proton transfer (ESIPT) in the *syn* form of MPP, 2) excited-state intermolecular double-proton transfer (ESDPT) in the dimers of PPP in nonpolar media, as well as 3) solvent-assisted double-proton transfer in hydrogen-bonded 1:1 complexes of PPP and MPP with alcoholic partners. The excited-state processes are manifested by the appearance of a dual luminescence and a bimodal irreversible kinetic coupling of the two fluorescence bands. Ground-state *syn–anti* equilibria are detected and discussed. The fraction of the higher-energy *anti* form varies for different derivatives and is strongly dependent on the solvent polarity and hydrogen-bond donor or acceptor abilities.

1. Introduction

Excited-state proton transfer (ESPT), one of the basic photochemical reactions, is of fundamental interest in chemistry and biology.[1–10] A particular attention is paid to heteroaromatic bifunctional molecules that can simultaneously act as hydrogen-bonding donors and acceptors and may reveal simultaneous enhancement of acidity and basicity upon electronic excitation, which provides a driving force for ESPT processes. The kinetics of these processes strongly depends on the geometrical structure and the strength of the hydrogen bonds. Photoinduced tautomerization in molecules with strong intramolecular hydrogen bonds is often an extremely rapid, barrierless or nearly barrierless process that can be detected even at very low temperatures under isolated solvent-free supersonic jet conditions. For instance, excited-state intramolecular proton transfer (ESIPT) has been observed in molecular beams for 2,5-bis(2′-benzoxazolyl)hydroquinone,[11] methyl salicylate,[12–16] salicylic acid,[17,18] *o*-hydroxyacetophenone and related systems,[16,19,20] and 2-(2′-pyridyl)pyrrole (PP).[21] On the other hand, a formation of intermolecular hydrogen-bonded bridges enables excited-state double-proton transfer (ESDPT) in dimers and alcohol and water complexes. This reaction has been observed for 7-azaindole,[22–25] 1-azacarbazole,[26–28] 2-(2′-pyridyl)indole and related compounds,[29–31] 1*H*-pyrrolo[3,2 h]quinoline,[32–40] and PP.[41] Among them, a particular class of azaaromatic compounds revealing NH/N tautomerization in hydrogen-bonded dimers—those mimicking the behaviour of nucleic base pairs[9,10,42–44]—has attracted considerable interest. The mechanism of the ESDPT process is being heavily discussed, in particular the issue of stepwise versus concerted movement of the protons.[10,45–47]

A special class of bifunctional molecules consists of compounds for which the proton-donor and -acceptor groups are located in separate moieties, linked by a single bond.[35,48] For this class of molecules, such as 2-(2′-pyridyl)indole and its isomers,[29–31,35] 2-(2′-pyridyl)pyrroles,[21,41,49,50] and 2-pyridylpyrazoles,[51] two rotameric structures are possible: 1) a *syn* form, with the donor and the acceptor on the same side, and 2) an *anti* species, with the two groups on opposite sides. Only the *syn* form is able to form cyclic, hydrogen-bonded complexes with water or alcohols. These complexes are efficiently deactivated in the lowest excited singlet state S_1, through internal conversion (IC) and/or proton transfer. Rotamerization results in a complete change of photophysical properties of the compounds since neither enhanced IC nor phototautomerization can occur in the *anti* form in protic media. 2-(2′-pyridyl)pyrrole is a rare example of a molecule that exhibits two types of photoreactions: 1) the ESIPT process in the bare molecule in non-

[a] *V. Vetokhina, M. Kijak, Prof. J. Waluk, Prof. J. Herbich*
Institute of Physical Chemistry, Polish Academy of Sciences
Kasprzaka 44/52, 01-224 Warsaw (Poland)
Fax: (+48) (22) 3433333
E-mail: herbich@ichf.edu.pl
waluk@ichf.edu.pl

[b] *Dr. K. Dobek*
Faculty of Physics, Adam Mickiewicz University
Umultowska 85, 61-614 Poznań (Poland)

[c] *I. I. Kamińska, Prof. J. Waluk, Prof. J. Herbich*
Faculty of Mathematics and Science
Cardinal Stefan Wyszyński University
Dewajtis 5, 01-815 Warsaw (Poland)

[d] *K. Muller, Prof. W. R. Thiel*
Kaiserslautern University of Technology
Erwin-Schrödinger-Str. 52, 67653 Kaiserslautern (Germany)

Supporting information for this article is available on the WWW under http://dx.doi.org/10.1002/cphc.201200602.

polar solvents[41] and under supersonic jet conditions,[21] and 2) the ESDPT reaction in hydrogen-bonded complexes with alcoholic partners.[41]

Herein, we focus on the solvent-dependent rotamerization (the question concerns the relative stability of various rotameric forms) and phototautomerization, exemplified by ESIPT in the especially synthesized series of 2-(1*H*-pyrazol-5-yl)pyridines (**2-PPs**): 2-(1*H*-pyrazol-5-yl)pyridine (**PPP**), 2-(3-methyl-1*H*-pyrazol-5-yl)pyridine (**MPP**), 2-(4-bromo-1*H*-pyrazol-5-yl)pyridine (**BPP**), and 2-(4-nitro-1*H*-pyrazol-5-yl)pyridine (**NPP**) (Scheme 1),

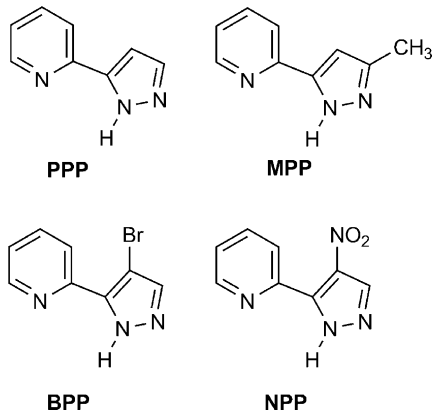

Scheme 1. Structures and acronyms of the investigated compounds.

and by ESDPT in their hydrogen-bonded dimers or complexes with protic partners. Thus, the effects of solute concentration, polarity, and hydrogen-bonding ability of the environment on the spectroscopic and photophysical properties of the solute (quantitative characterization of the electronic structure, ground- and excited-state dipole moments, radiative and radiationless transitions and the structural changes) are examined and discussed. A related aim of this work is to study the effects of electron-withdrawing (–Br, $-NO_2$) or electron-donating ($-CH_3$) substituents on the spectroscopy and luminescence properties of these **2-PPs**.

Methods

Experimental Section

The synthesis of the compounds was described previously.[52–55]

The solvents used for our studies, *n*-hexane (HEX), ethyl acetate (EA), acetonitrile (ACN) and the alcohols 1-propanol (1-PrOH) and 1-butanol (1-BuOH), were of spectroscopic or fluorescence grade (Aldrich or Merck). Water was used after four distillations over $KMnO_4$ in a quartz apparatus. All solvents were carefully checked prior to the measurements and showed no residual emission.

Electronic absorption spectra were recorded on Shimadzu UV 2401 and Shimadzu UV 3100 spectrophotometers. Stationary fluorescence and fluorescence excitation spectra were measured on an Edinburgh FS 900 CDT fluorometer and with the Jasny multifunctional spectrofluorimetric system.[56] The spectra were corrected using the spectral sensitivity curves of the instruments. Fluorescence spectra were recorded as a function of the wavelength (λ) and subsequently multiplied by a factor of λ^2 in order to convert counts per wavelength into counts per wavenumber. For the quantum-yield determinations, the solutions had identical optical densities at the excitation wavelength. Quinine sulphate in 0.05 mol dm^{-3} H_2SO_4 ($\Phi_f = 0.51$)[57] and 4-dimethylaminopyridine in acetonitrile ($\Phi_f = 0.017$)[58] served as references for fluorescence quantum-yield determination. Fluorescence lifetimes in the subnanosecond range were measured on an Edinburgh FL 900 CDT time-resolved fluorometer, with an estimated time resolution of about 500 ps. The time-resolved single-photon-counting technique was used, followed by data reconvolution using the non-linear least squares fitting routine.

Time-resolved fluorescence decays in the picosecond range were measured using a time-correlated single-photon-counting system (TCSPC).[59] An 82 MHz train of 840 nm pulses of 1–2 ps half-width was delivered by a Ti:Sapphire "Tsunami" (Spectra-Physics) laser pumped by a Millennia Prime (Spectra-Physics) cw laser. The frequency of the pulses train was decreased to 4 MHz by a pulse-selector (3980-2S, Spectra-Physics) and next, frequency tripled to 280 nm by a harmonic generator (GWU-23PS, Spectra-Physics). The pump pulses were focused by a 200 mm focal-length aspheric lens into a crystal quartz cuvette of 2 mm optical path, filled with the sample solution. The fluorescence was accumulated in the TCSPC regime perpendicularly to the excitation direction using a TCC900 (Edinburgh Instruments) detection system equipped with a thermoelectrically cooled microchannel plate-photomultipler tube R3809U-05 (Hamamatsu). The emission monochromator had entrance and exit slits set to 9 nm of spectral width. The TCC900 multichannel analyzer time per channel was set to 0.61 ps and the fluorescence decays were accumulated into 4096 channels. An instrumental response function (IRF) of 30 ps full-width at half of the maximum (FWHM) was determined by measuring the scattered signal from Ludox in water solution. This signal was also applied in the multiexponentional reconvolution approximation method used in the analysis of decays, with the minimization performed by the downhill simplex algorithm.

Computations

All the ground-state computations were performed with the Gaussian 03 suite of programs.[60] Ground-state geometry optimizations were carried out at the density functional (DFT) level of theory, using the B3LYP hybrid functional and 6-31+G(d,p) basis set. The basis-set superposition error (BSSE) was corrected by the counterpoise technique.[61,62] For calculations including the presence of a solvent the polarizable continuum model (PCM) was used.[63,64] The united-atom topological model (UAHF) with the ALPHA scaling factor equal to 1.2 was applied.[65] Vertical excitation energies were obtained with the time-dependent DFT method (TDDFT). For stationary points, the Hessian matrix was calculated and diagonalized to check whether the points correspond to minima.

2. Results and Discussion

2.1. Tautomeric/Rotameric Forms

Formally, the compounds under study can exist in six different tautomeric/rotameric (T/R) forms, either one of three tautomers *syn*, *syn1*, and *taut* or one of three corresponding rotameric forms *anti*, *anti1*, and *taut1* (Scheme 2). According to previous theoretical and experimental NMR and IR investigations in solutions, the *syn* form is the major T/R form in the

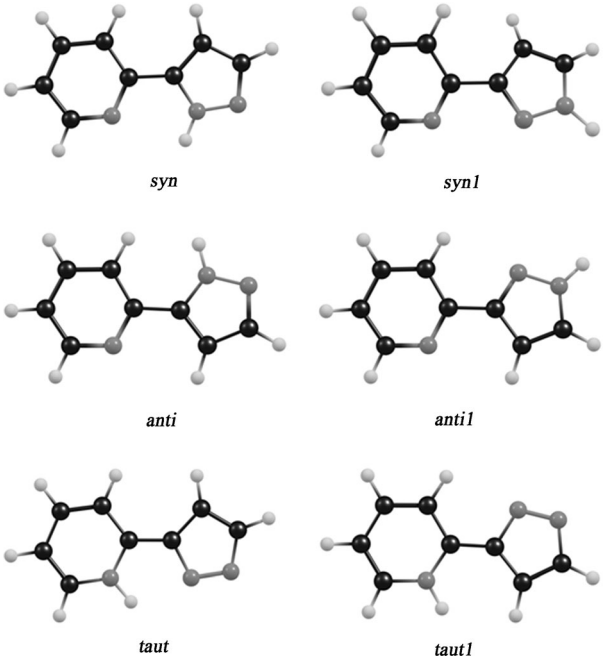

Scheme 2. Various rotameric/tautomeric forms of 2-(1*H*-pyrazol-5-yl)pyridine (**PPP**).

ground state of **PPP**, **MPP**, **BPP**, and **NPP**.[52] IR experiments in dichloromethane show only one N–H absorption band at about 3400 cm^{-1} for all compounds (except for **MPP** which reveals also the second band at 3511 cm^{-1}) assigned to the *syn* form. Our theoretical predictions (Table 1) of relative energies of the various forms of **2-PPs** are in agreement with the previous results. The *syn* form is expected to be a dominant R/T form for all the studied molecules under vacuum isolation conditions. In a polar environment (e.g. in acetonitrile), however, in spite of the markedly lower value of the ground-state dipole moment of the *anti1* form with respect to the *syn* one (Table 2), the former is relatively stabilized and the fraction of the *anti1* rotamer significantly increases from 0.09 to 0.26 for **PPP**, from 0.07 to 0.37 for **MPP**, and from 0.00 to 0.07 for **BPP**. The calculations predict for these compounds at room temperature only a small fraction of about 1–4% of the other ground-state rotameric forms in aprotic polar media due to the relatively high energies of the *syn1* and *anti* forms. For **NPP**, however, the increase of the environmental polarity leads to significant fractions of *anti*, *anti1*, and *syn1* forms: 0.16, 0.14, and 0.11, respectively.

2.2 Electronic Absorption

Solvent effects on the room-temperature electronic-absorption spectra of 2-(1*H*-pyrazol-5-yl)pyridines (**2-PPs**) are shown in Figure 1. The experimental and TDDFT-computed absorption data are collected in Table 2.

The near-UV absorption spectrum of **PPP** in HEX shows two bands. The first one is centered at 287.5 nm (~34780 cm^{-1}) and the second one at 256 nm (~39060 cm^{-1}). A similar spectral pattern is observed for **MPP** and **BPP**. In contrast, **NPP** shows three absorption bands in this spectral region. The two lowest absorption bands are red-shifted by about 1500 cm^{-1} with respect to those of the other compounds studied. Interestingly, the ratios of the molar absorption coefficients $\varepsilon_1/\varepsilon_2$ of the two lowest absorption bands of **BPP** and **NPP** in HEX are significantly higher than those of **PPP** and **MPP**. These findings are in agreement with

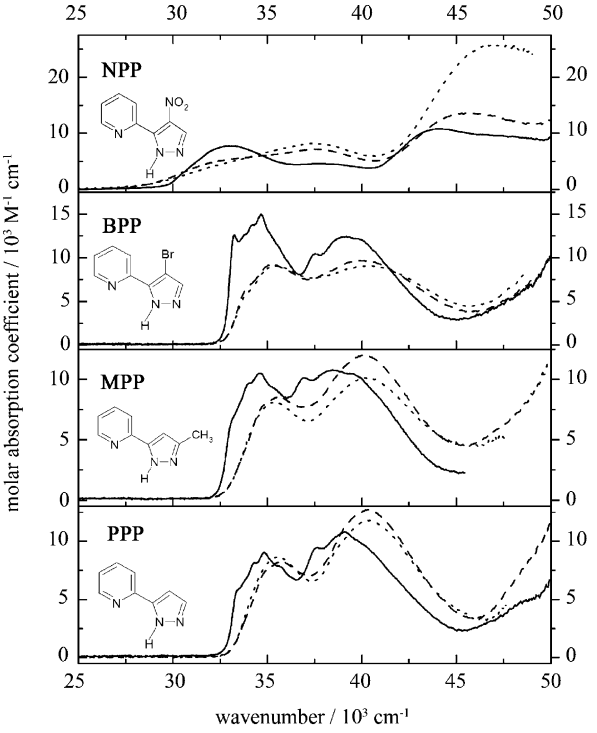

Figure 1. Room-temperature absorption spectra of **PPP**, **MPP**, **BPP**, and **NPP** in HEX (——), ACN (-----), and 1-PrOH (•••••). *M* [mol dm^{-3}].

Table 1. B3LYP/6-31G(d,p)/ZPE relative energies (in kcal mol^{-1}) and estimated fractions (f_{est})[a] of the various forms of **PPP**, **MPP**, **BPP**, and **NPP**, either under vacuum-isolation conditions or in ACN.[b]

Compound		*syn* energy	(f_{est})	*syn1* energy	(f_{est})	*anti* energy	(f_{est})	*anti1* energy	(f_{est})
PPP	vacuum	0.00	0.91	6.05	0.00	3.58	0.00	1.37	0.09
	ACN	0.00	0.68	2.11[a]	0.02	1.63[a]	0.04	0.57[a]	0.26
MPP	vacuum	0.00	0.93	6.27	0.00	3.55	0.00	1.56	0.07
	ACN	0.00	0.57	1.79[a]	0.03	1.57[a]	0.04	0.26[a]	0.37
BPP	vacuum	0.00	1.00	7.60	0.00	5.70	0.00	4.01	0.00
	ACN	0.00	0.92	2.86[a]	0.01	2.70[a]	0.01	1.56[a]	0.07
NPP	vacuum	0.00	1.00	7.00	0.00	6.30	0.00	6.12	0.00
	ACN	0.00	0.59	1.00[a]	0.11	0.79[a]	0.16	0.86[a]	0.14

[a] According to the Boltzmann distribution. [b] The polarizable continuum model (PCM) is used.

Table 2. Comparison between vertical TDDFT excitation energies ($\tilde{\nu}_{TDDFT}$, in $10^3\,cm^{-1}$) of the low-lying $S_0\rightarrow{}^1(\pi,\pi^*)$ transitions and oscillator strengths (f) for various forms of **2-PPs** studied (the energies of the low-lying $S_0\rightarrow{}^1(n,\pi^*)$ excitations are not included in the Table), as well as the locations of the experimental bands ($\tilde{\nu}_{exp}$, in $10^3\,cm^{-1}$) and molar absorption coefficients (ε, in $dm^3\,mol^{-1}\,cm^{-1}$) of the near-UV absorption-band maxima in HEX.

Compound	form		TD-DFT/B3LYP/6-31+G(d,p) $\tilde{\nu}_{TDDFT}$[a]	f	μ[b]	Experimental $\tilde{\nu}_{exp}$	ε
PPP	*syn*	S_0			4.1		
		S_1	35.69	0.2769	3.5	34.78	10800
		S_2	37.94	0.2197	2.8	39.06	12770
		S_3	40.19	0.0203	4.4		
	anti1	S_0			1.6		
		S_1	38.63	0.2272	5.4		
		S_2	40.45	0.1990			
		S_3	42.59	0.0107			
MPP	*syn*	S_0			3.7		
		S_1	35.24	0.2859	5.8	34.60	10880
		S_2	37.21	0.0988		38.54	11160
		S_3	38.22	0.1592			
	anti1	S_0			2.0		
		S_1	38.31	0.2323	7.0		
		S_2	39.94	0.1971			
		S_3	40.83	0.0084			
BPP	*syn*	S_0			3.7		
		S_1	34.88	0.2879	4.7	34.66	12940
		S_2	37.95	0.0247		39.14	10770
		S_3	38.78	0.1615			
	anti1	S_0			2.6		
		S_1	37.49	0.2224	8.1		
		S_2	39.36	0.0225			
		S_3	41.32	0.1813			
NPP	*syn*	S_0			5.5		
		S_1	30.93	0.2238	10.3	33.11	10350
		S_2	37.24	0.1227		37.59	5920
		S_3				44.05	14500
	anti1[c]	S_0			5.2		
		S_1	32.48	0.0476	12.8		
		S_2	39.57	0.0626			
	syn1[c]	S_0			3.4		
		S_1	29.29	0.0175	6.5		
		S_2	31.62	0.0183			
		S_3	38.43	0.0593			
	anti[c]	S_0			6.8		
		S_1	34.51	0.0308	9.1		
		S_2	31.62	0.0183			
		S_3	38.43	0.0593			

[a] B3LYP/6-31+G(d,p) optimized ground-state conformations are used as input geometries. [b] Dipole moments in debyes. [c] Due to the lack of the planar structure of the *anti1*, *syn1*, and *anti* forms of NPP the strict distinction between $^1(\pi,\pi^*)$ states and $^1(n,\pi^*)$ states is not possible. Only transitions of significant intensity are shown.

the results of TDDFT/B3LYP/6-31+G(d,p) computations. The calculated energies of transitions to the low-lying excited $^1(\pi,\pi^*)$ states of the *syn* tautomers of **PPP**, **MPP**, and **BPP** are in an excellent agreement with the experimentally measured absorption maxima (Table 2). The largest discrepancies do not exceed 1300 cm^{-1} for the $S_0\rightarrow S_1$ and $S_0\rightarrow S_i$ transitions ($i=2$ or 3 correspond to the computed transitions carrying higher oscillator strengths). The discrepancy for the lowest energy transition for **NPP** is about 2200 cm^{-1}. In agreement with experimental observations, the calculated spectral positions and oscillator strengths f_1, f_2, and f_3, of the three lowest $S_0\rightarrow{}^1(\pi,\pi^*)$ vertical transitions lead to the higher relative intensity of the first computed absorption band for the *syn* forms of **NPP** and **BPP** than for **PPP** and **MPP** (see the Supporting Information, Figure S1).

The spectra reveal a significant blue shift and a decrease in relative intensity of the lowest absorption band compared to that of the second one with increasing solvent polarity and hydrogen-bond donor or acceptor ability. The latter effect is particularly pronounced for **NPP**. This finding is opposite to that expected on the basis of interactions between close-lying $^1(\pi,\pi^*)$ and $^1(n,\pi^*)$ states [the vertical transitions to the lowest $^1(n,\pi^*)$ states are computed to lie higher than those to the lowest $^1(\pi,\pi^*)$ states of about 2800 cm^{-1}, 3300 cm^{-1}, and 3300 cm^{-1} for the *syn* forms of **PPP**, **MPP**, and **BPP**, respectively], which can decrease the electronic transition dipole moments in nonpolar media (proximity effect),[66] as the increase of solvent polarity should destabilize the $^1(n,\pi^*)$ states relative to the $^1(\pi,\pi^*)$ states. The most plausible explanation involves the solvent-dependent coexistence of various tautomeric forms of **2-PPs** in the ground state. The TDDFT calculations for the *syn* forms of all the compounds under study predict that, upon excitation to the lowest $^1(\pi,\pi^*)$ state, the dipole moment decreases (**PPP**) or increases (**MPP, BPP**, Table 2) and its direction is nearly reversed (see the Supporting Information, Figure S2). Such a situation should lead to a blue shift of the lowest absorption band of **PPP**, **MPP**, and **BPP** in polar solvents. Moreover, according to the DFT/B3LYP/6-31+G(d,p)-PCM calculations, the increase in solvent polarity should result in an appearance and rise of the fraction of the *anti1* tautomer of **PPP**, **MPP**, and **BPP** as well as the *anti*, *anti1*, and *syn1* forms of **NPP** (Table 1). The calculations predict, in agreement with the experimental findings, that the lowest absorption transitions for the *anti1* forms of **PPP**, **MPP**, and **BPP** should be considerably blue-shifted by about 2600–3000 cm^{-1} with respect to those of the *syn* forms. For **NPP**, the oscillator strengths corresponding to the lowest $S_0\rightarrow S_1$ transitions for the *anti*, *anti1*, and *syn1* forms are computed to be about one order of magnitude lower than that for the *syn* rotamer (Table 2). This should lead to a dramatic decrease in intensity of the lowest absorption band for **NPP**, which is indeed observed.

2.3. Fluorescence

Room-temperature fluorescence spectra of **PPP**, **MPP**, and **BPP** recorded in nonpolar (HEX), medium polar aprotic (EA), strongly polar aprotic (ACN), and polar protic (1-PrOH, water) solutions are presented in Figure 2. The compounds show a dual luminescence in HEX, 1-PrOH, and water. The dominant short-wave fluorescence is accompanied by a second band (shoulder in aqueous solutions) of a very weak intensity, which appears at much lower energies. The shifts between the maxima of the two emissions vary from about 10000–11000 cm^{-1} for **PPP** and **BPP** to about 12000–14000 cm^{-1} for **MPP** in HEX and 1-PrOH, respectively. In highly polar aprotic media, such as ACN, only a trace of the low-energy band is observed. The short-wave fluorescences of **MPP** and **PPP** exhibit similar responses

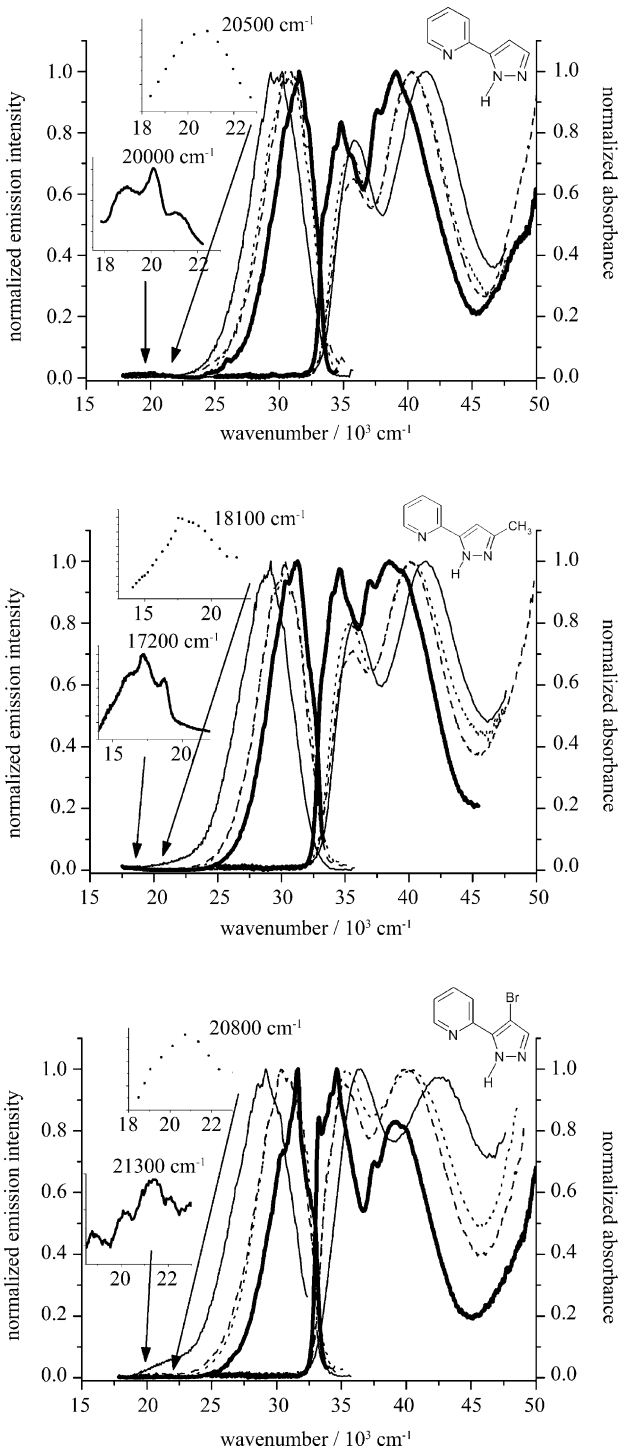

Figure 2. Room-temperature absorption and fluorescence spectra of **PPP** (top), **MPP** (middle), and **BPP** (bottom) in HEX (——), ACN (- - - -), 1-PrOH (·····), and in aqueous solutions (——). The spectra in EA are similar to those in ACN. The insets show the low-energy emission bands observed for the compounds in HEX (lower panel) and 1-PrOH (higher panel). The latter spectra are smoothed using the Savitzky–Golay method implemented in the Origin 8.0 software.

to a change from aprotic to protic solvents. The values of the quantum yields Φ_f significantly increase in alcohols and water (Table 3). The Φ_f values of this emission for **MPP** (varying with the solvent from 8×10^{-3} in ACN to 4.5×10^{-2} in H_2O) and **PPP** (3×10^{-3} in ACN and 3.5×10^{-2} in H_2O) are higher than those determined for **BPP**, which reveals a very weak fluorescence with a quantum yield close to 10^{-3} in various media. The emission of **NPP**, if any, was below the detection limit of our spectrofluorimeters. This finding is in agreement with the results of TDDFT computations which predict that the energy of the vertical transition to the lowest $^1(n,\pi^*)$ state of the *syn* form of **NPP** is lower by about 1170 cm^{-1} than that of the lowest $^1(\pi,\pi^*)$ state.

The excitation spectra of both fluorescence bands of **PPP** and **MPP**[51] in HEX (Figure 3) match well the corresponding absorption spectra (interestingly, a small discrepancy is observed for **PPP** at the red edge of the excitation spectrum for the low-energy emission). Contrary to the behaviour in a nonpolar medium, the excitation spectra of the short-wave emission in ACN do not coincide with the absorptions. The relative intensity of the lowest band in the excitation spectrum is significantly higher than that in the absorption spectrum. Moreover, the excitation spectra are slightly shifted to lower energies. A similar, but smaller effect is observed for **BPP**. Taking into account the coexistence of the *syn* and *anti1* forms of the compounds in the polar environment (Table 1), and in accordance with the theoretical predictions that the lowest absorption transitions for the *anti1* forms of **PPP**, **MPP**, and **BPP** should be considerably blue-shifted by about 2600–3000 cm^{-1} with respect to those of the *syn* forms, this finding indicates that the short-wave fluorescence originates mainly from the *syn* rotamer. The excitation spectra of the short-wave emission in 1-PrOH, similarly to ACN, show a relative increase of the low-energy excitation band with respect to that in the absorption spectra. The maximum of the lowest excitation band, however, is now slightly shifted to higher energies. Contrary to that, the lowest excitation band of the low-energy emission of **PPP**, **MPP**, and **BPP** (not shown) is markedly shifted to the red. According to the results of theoretical computations this effect is expected in all the **2-PPs** studied for the complexes of the *syn* form with an alcohol molecule.

2.4. Acid–Base Equilibria

The spectral location of the low-energy fluorescence in HEX, 1-PrOH, and in aqueous solutions is similar to that previously observed for **MPP** in cyclohexane[51] and for PP in nonpolar and protic media.[41] Therefore, in accordance with previous investigations, this band is assigned to a tautomeric species which is formed either in the ESIPT or in the ESDPT reaction. The driving force for the excited-state proton transfer is an increase in the excited-state pK_a of the proton acceptor and a decrease in the excited-state pK_a of the proton donor. Changes of pK_a in the excited state can be obtained from the Förster cycle,[67,68] employing Equation (1):

$$pK_a^* \approx pK_a + \frac{Nhc}{2.303R}\frac{(\tilde{\nu}_B - \tilde{\nu}_{BH^+})}{T} \quad (1)$$

where pK_a^* and pK_a denote the values in the excited and ground state, respectively. *N*, *h*, *c*, *R*, and *T* are the Avogadro

Table 3. Solvent effects on the spectral position of the short-wave fluorescence maxima ($\tilde{\nu}_{fl}$), quantum yields (Φ_f), decay times (τ), and resulting radiationless (k_{nr}) and radiative (k_f) rate constants, and electronic transition dipole moments M_{fl}. $\tilde{\nu}_{TDDFT}$ denote TDDFT/B3LYP/6-31+G(d,p) energies of the $^1(\pi,\pi^*)\rightarrow S_0$ emission of the *syn* and *anti1* forms under vacuum isolation conditions. The calculations were carried out for the excited-state equilibrium geometries.

Compound	Solvent	$\tilde{\nu}_{TDDFT}$ *syn* [cm^{-1}]	$\tilde{\nu}_{TDDFT}$ *anti1* [cm^{-1}]	$\tilde{\nu}_{fl}$[a] [cm^{-1}]	Φ_f	τ [ps]	k_{nr} 10^{10} s^{-1}	k_f 10^8 s^{-1}	M_{fl} [D][c]
PPP	HEX	31130	34710	31500	0.008[b]	42[b]	2.4	~1.9	~2.7
	EA			31000	~0.004				
	ACN			31000	~0.003	19(±5)	~5.2	~1.6	~2.7
	1-PrOH			30600	0.017[b]	[*m-ex]			
	H_2O			29800	0.035[b]				
MPP	HEX	29250	34200	31100	0.018[b]	84[b,**]	1.2	2.1	2.9
	EA			30200	0.012[b]				
	ACN			30200	0.008[b]	68[b,d]	1.5	1.2	2.4
	1-PrOH			30100	0.028[b]	[*m-ex]			
	H_2O			29100	0.045[b]				
BPP	HEX	30125	32190	31600	~0.003	16(±5)[e] 45[b,e]			
	EA			30700	~0.003				
	ACN			30700	~0.003	16(±5)	~6.2	~1.9	~2.9
	1-PrOH			30700	~0.002	[*m-ex]			
	H_2O			29200	~0.003				

[a] Scatter of results: ±150 cm^{-1}. [b] Error is about 10%. Thus, the maximum error is about 20% for the rate constants k_{nr} and k_f and about 10% for the transition moment M_{fl}. [c] In debyes. [d] The dominant component (see text). [e] Biexponential decay (contributions: 60% and 40%, respectively). [*m-ex] multiexponential decay. [**] 115 ps in ref. [51].

number, the Planck constant, the speed of the light, the gas constant, and the temperature.

The procedure was applied for the spectra of neutral and protonated molecules. From the absorption and fluorescence of these species, the 0–0 transitions of both forms ($\tilde{\nu}_B$ and $\tilde{\nu}_{BH^+}$) can be estimated, yielding ΔpK_a, the change in pK_a upon $S_0\rightarrow S_1$ excitation. The values (Table 4) are huge and similar to that of PP ($\Delta pK_a \cong +11.0$).[41] These findings leave no doubts that the protonation centre in the **2-PPs** studied is the pyridine nitrogen atom. It is interesting that the highest basicity increase is observed for **MPP**, a derivative substituted with an electron-donating methyl group.

Table 4. The 0–0 transition energies obtained from the absorption and fluorescence maxima of the neutral ($\tilde{\nu}_B$, in ACN) and protonated ($\tilde{\nu}_{BH^+}$)[a] forms and the resulting pK_a changes in the S_1 state, for protonation on the pyridine nitrogen atom.

Compound	$\tilde{\nu}_B$ [cm^{-1}]	$\tilde{\nu}_{BH^+}$ [cm^{-1}]	$\Delta pK_a = pK_a^* - pK_a$
PPP	33120	29520	7.5[b]
MPP	32980	27600	11.3[b]
BPP	33000	29230	7.9[b]
NPP	~33700	~30600	~6.5[b]

[a] Protonation was achieved by adding about 0.1 mol dm^{-3} of $HClO_4$. [b] Estimated from Equation (1).

2.5. Spectrophotometric Titration

In order to explain the origin of the long-wave fluorescence band in alcohols, titration experiments have been performed. Upon addition of 1-butanol (or 1-PrOH), at concentrations low enough to prevent the formation of alcohol oligomers,[29] to a solution of **PPP** in HEX, spectral changes are seen, both in absorption and emission (Figure 4). In the absorption spectra an isosbestic point is observed. Assuming the presence of two species, a bare molecule and a complex with alcohol, the absorption data yield a 1:1 stoichiometry of the complex and an equilibrium constant of $K \cong 35(\pm 3)$ $dm^3\,mol^{-1}$. In emission, the decrease of the short-wave fluorescence is accompanied by the growth of the tautomeric band. Noticeably, the intensities of both emission bands for **PPP**, contrary to bulk alcoholic solutions (Figure 2), become similar for a concentration of 1-BuOH of about 3.6×10^{-2} mol dm^{-3}. This interesting finding can be explained by the formation of mainly one type of the ground-state complex between **PPP** and 1-BuOH (or 1-PrOH), capable of phototautomerization. The 1:1 stoichiometry of the complex and the relatively efficient low-energy fluorescence suggest its structure. At low alcohol concentrations a cyclic, doubly hydrogen-bonded complex of the *syn* form of **PPP** with the alcoholic partner seems to be formed. Titration of **MPP** and **BPP** in HEX with 1-BuOH also reveals the formation of 1:1 complexes with equilibrium constants of $K \cong 50(\pm 7)$ $dm^3\,mol^{-1}$ and $K \cong 13(\pm 3)$ $dm^3\,mol^{-1}$. However, the intensity of the low-energy emission, which increases with the increasing concentration of alcohol in the range from 0.0036 to 0.072 mol dm^{-3}, is relatively weak. In bulk alcohol solutions, an extremely weak intensity of the low-energy fluorescence is a consequence of the existence of other solvates of various geometries and stoichiometries, which are unable to tautomerize.[29,34,41] Interestingly, the intensity of the tautomeric emission of **BPP** and **MPP** in aqueous solutions, contrary to that in 1-PrOH, is higher than that of **PPP** (Figure 2). **PPP** in water shows only a trace of the low-energy emission.

2.6. Picosecond Kinetics

The assignment of the low-energy fluorescence band of **PPP**, **MPP**, and **BPP** in HEX is more ambiguous than that in alcohols. The calculations and the nuclear Overhauser effect spectrosco-

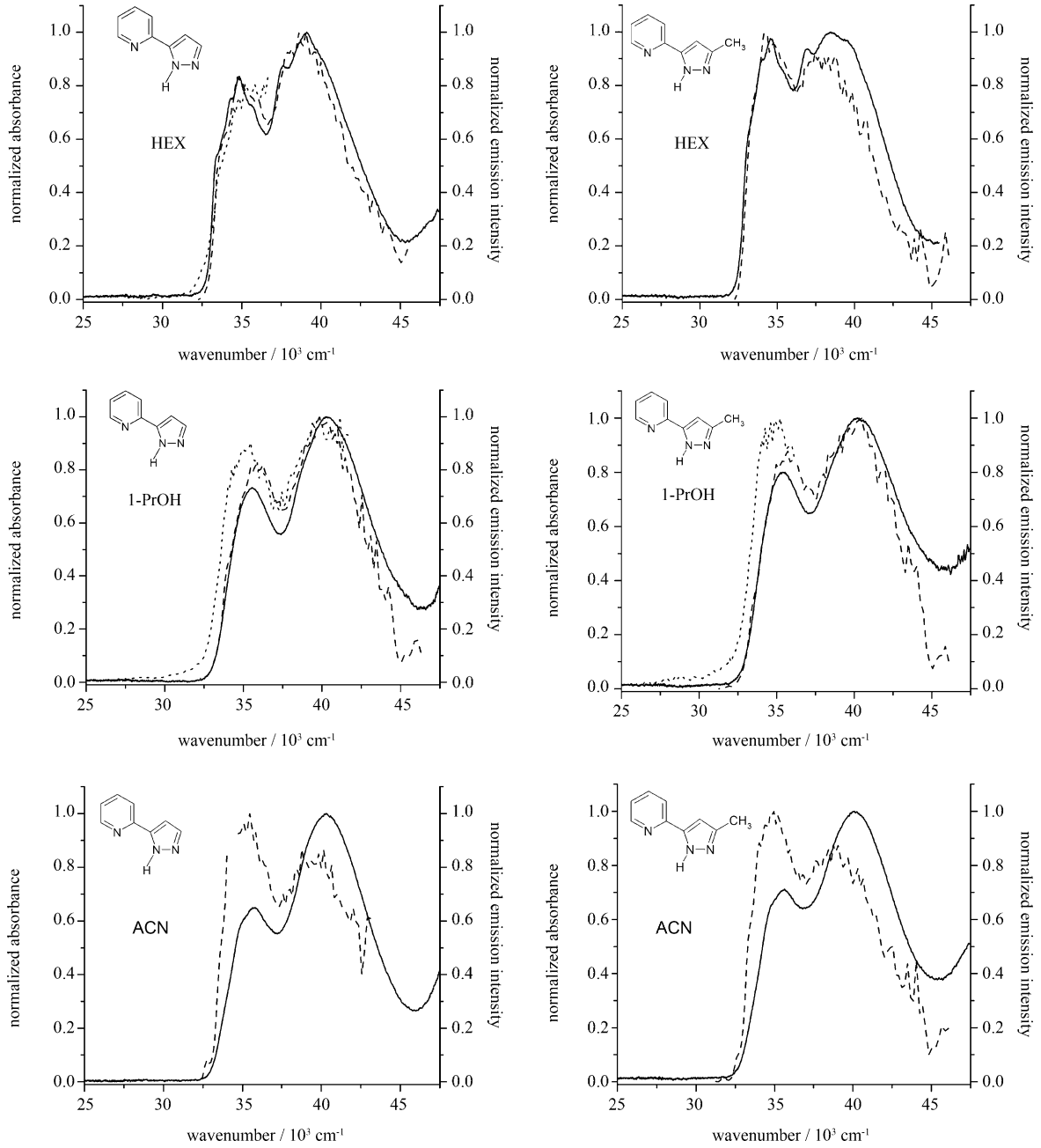

Figure 3. Room-temperature absorption (——) and fluorescence excitation spectra of **PPP** (left) and **MPP** (right) monitored at 33 300 cm^{-1} (-----) and at 20 000 cm^{-1} (••••). Upper panel, HEX; middle panel, 1-PrOH; lower panel, ACN.

py (NOESY) investigations performed for 3,5-dimethyl-2-(2′-pyridyl)pyrrole[49] suggest the existence of hydrogen-bonded dimers of the *syn* forms in the ground state. Such dimers should be doubly hydrogen-bonded in a cyclic fashion. Our theoretical calculations [at the B3LYP/6-31 + G(d,p) level including BSSE and zero-point vibrational-energy (ZPE) corrections] predict a slightly higher stabilization energy for the ground-state dimers of **PPP** and **MPP** (6.8 kcal mol^{-1} and 6.6 kcal mol^{-1}, respectively) than for **PP** (5.8 kcal mol^{-1}). The calculated value for **BPP** is 5.5 kcal mol^{-1}. In order to gain more insight into the origin of both emissions, kinetic studies were performed. The fluorescence kinetic data obtained on the nanosecond time scale for **PPP** in HEX showed a biexponential decay of the long-wave fluorescence band, with the longer component of about 1 ns. The lifetimes of the high-energy fluorescence of **PPP**, **MPP**, and **BPP** in various media, however, were too short to be measured with subnanosecond resolution. We therefore carried out picosecond kinetic studies in HEX, acetonitrile and in mixed HEX + 1-PrOH solvent at room temperature.

The solvent polarity effects on the spectral position of the short-wave fluorescence maxima ($\tilde{\nu}_{fl}$), quantum yields (Φ_f), and decay times (τ) of these **2-PPs** are collected in Table 3. More information about the nature of the radiative transitions can be obtained from the analysis of the fluorescence rate constants

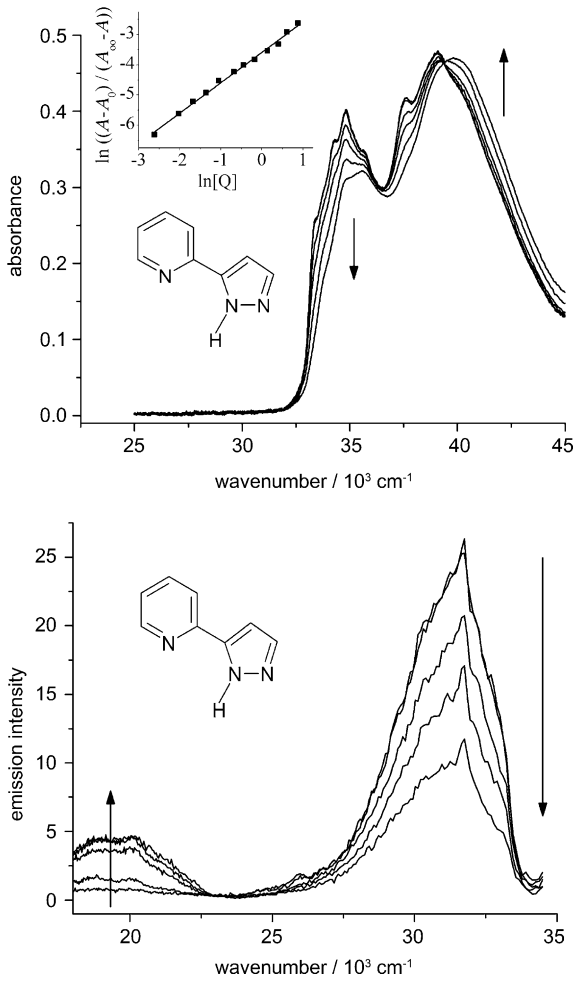

Figure 4. Titration of **PPP** solution in HEX with 1-BuOH at 293 K. Changes in absorption (top), evolution of both fluorescence bands (bottom). The arrows show spectral changes accompanying the addition of alcohol. The alcohol concentration varied from 0.0036 to 0.072 mol dm^{-3}. The inset in the absorption part shows the determination of the equilibrium constant and stoichiometry of the complex from the absorption data recorded at 37600 cm^{-1}. A_0 and A_∞ denote the absorbance measured when only the bare or complexed forms are present, and A is the absorbance measured at an alcohol concentration [Q], see Equations (1), (2), and (6) in ref. [30].

k_f and the electronic transition dipole moments M_{fl} (being the best quantitative measure of the transition probability). In the electric dipole approximation, the M_{fl} values can be determined from the radiative (k_f) rate constants which are related to the fluorescence quantum yields (Φ_f) and lifetimes τ by Equation (2):

$$k_f = \Phi_f/\tau, \qquad (2)$$

and the resulting values of M_{fl} are given by Equation (3):[69,70]

$$k_f = \frac{64\pi^4}{3h}(n\tilde{\nu}_{fl})^3\left|\vec{M}_{fl}\right|^2 \qquad (3)$$

where n is the refractive index of the solvent.

The kinetics of the short-wave fluorescence, excited at 35700 cm^{-1} and monitored at 30800 cm^{-1}, of **MPP** and **PPP** in HEX and of **PPP** in ACN at 293 K could be satisfactorily fitted to a monoexponential decay (Table 3). Variations of the excitation between 33300 cm^{-1} and 35700 cm^{-1} and monitoring the emission spectral region between 27750 cm^{-1} and 31250 cm^{-1} did not change the results. Our experiments, however, cannot definitively exclude a small contribution (less than 7%) of very short-lived components [~10(±5) ps] for **PPP** and **MPP** in HEX. The decay of the fluorescence of **MPP** in ACN involves two components: $\tau_1 \cong 68$ ps and $\tau_2 \cong 18$ ps with contributions of about 91% and 9%, respectively. The obtained lifetimes of 84(±8) ps and 42(±4) ps for the dominant forms of **MPP** and **PPP** in HEX and 68(±7) ps and 19(±5) ps for **MPP** and **PPP** in ACN, respectively, lead to large values of the fluorescence rate constants $k_f > 10^8$ s^{-1}. Similarly high k_f values have been experimentally determined for the *syn* rotamers of 2-(2′-pyridyl)indole[35] and related compounds,[48] and 2-(2′-pyridyl)pyrrole.[48] Noticeably, the fluorescence lifetimes attributed to the *anti* rotamers were much longer (e.g. for PP: $\tau_{syn} \cong 33$ ps in HEX[48] and $\tau_{anti} \cong 4.6$ ns in ACN[41]). Thus, the results of our kinetic studies indicate, in agreement with the results of the photostationary investigations, that the short-wave fluorescence of **PPP** and **MPP** in aprotic media originates from the *syn* forms. The lack of the emission from the *anti1* form is in agreement with the results of calculations which predict the lowest S_1 state of n,π* character in this form.

The decay of the short-wave fluorescence of **BPP** in HEX, contrary to that in ACN (Table 3), involves two components: $\tau_1 \cong 16(\pm 5)$ ps and $\tau_2 \cong 45(\pm 5)$ ps with comparable contributions of about 60% and 40%, respectively. According to the results of the photostationary investigations and theoretical predictions this finding can hardly be explained in terms of the coexistence of the two rotameric forms *syn* and *anti1*. The concentration-dependence experiments do not show any significant changes of the relative contributions (the contribution of the short-lived component increases, however, by a few percent with the increase of the **BPP** concentration between 2.5×10^{-5} mol dm^{-3} and 3×10^{-3} mol dm^{-3}). The experiments performed for HEX containing very small contamination of water cannot exclude definitively that one of the decay components is connected with the complexes between **BPP** and water impurities in HEX. It should be stressed here, that the detailed analysis of the dependence of the kinetic curves of the long-wave fluorescence band on the UV-irradiating time (280 nm) suggests that **BPP** in HEX, contrary to **PPP** and **MPP**, undergoes a photochemical reaction under conditions of picosecond kinetic studies. The appearance of the photochemical product significantly increases the intensity of the low-energy fluorescence, but does not lead to any significant changes in the photostationary absorption and short-wave fluorescence spectra, as well as in the short-wave fluorescence kinetics.

The picosecond kinetic studies of **MPP** in HEX confirm the previously published[51] bimodal irreversible kinetic coupling of both fluorescence bands. The 84 ps lifetime of the high-energy fluorescence is recovered in the rise of the low-energy emission, which decays in 105 ps (Table 5). The ratio of the amplitudes of both kinetic components being about −1.0 proves that both fluorescence bands have the same precursor in the

Table 5. Dual fluorescence kinetics: characteristic decay (τ_{decay}, in ps) and rise (τ_{rise}, in ps) times for the short-wave (monitored at 325 nm) and long-wave fluorescence (monitored at 540 nm) of **PPP** and **MPP** in HEX and in a mixed solvent (HEX + 1-PrOH, concentration[*] of alcohol $c - 8.8\times10^{-2}$ mol dm^{-3}). The long-wave fluorescence in ACN was too weak to be measured.

Compound	Solvent[a]	325 nm τ_{decay}	540 nm τ_{rise}	540 nm τ_{decay}	540 nm τ_{decay}
PPP	HEX	42[a]	16(±5)[b]	1400[a,*]	380
	HEX + 1-PrOH	~21 (40%)[c]	18(±5)	630[a]	
		~55 (37.5%)[c]	(−0.99)[d]	(1.0)[d]	
		~213 (22.5%)[c]			
MPP	HEX	84[a]	84[a]	105[a]	
			(−0.92)[d]	(1.0)[d]	
	HEX + 1-PrOH	~18 (22%)[c]	16(±5)	280[a]	~990
		~76 (50%)[c]	(−1.0)[d]	(0.92)[d]	(0.02)[d]
		~200 (28%)[c]			
BPP	HEX	16(±5)[e]	[f,*]		
		45[a,e]			
	HEX + 1-PrOH	[m-ex],[*]	[f,*]		

[a] Error is about 10%. [b] The contribution of this component is very small for the small concentration of the solute of about 1×10^{-5} mol dm^{-3}. [c] In the brackets are the relative contributions of the respective decay times. [d] In the brackets are the amplitudes (in arbitrary units) of the corresponding rise and decay times. [e] Biexponential decay (contributions: 60% and 40%, respectively). [m-ex] Multiexponential decay. [f] The long-wave fluorescence of **BPP** in HEX corresponds in part to the product of photochemical reaction which happens under experimental conditions of the picosecond kinetic studies. [*] See text for explanation.

ground state. The kinetic studies do not reveal any concentration dependence. Thus, high- and low-energy emission bands are assigned to the *syn* and *taut* forms of the bare **MPP** molecule, respectively (Scheme 2 and 3).

On the other hand, the 42 ps decay of the short-wave fluorescence of **PPP** in HEX is not recovered in the rise of the long-wave band (Table 5). The decay of the long-wave band is biexponential and characterized by the lifetimes of about 1.4 ns and 380 ps. The concentration-dependence experiments show that the relative contribution of the longer component increases from 25% to 87% with the increase of **PPP** concentration from 1.2×10^{-5} mol dm^{-3} to 5×10^{-4} mol dm^{-3} (Figure 5). These findings leave no doubts that both emission bands of **PPP** in HEX originate from different species. The dominant short-wave emission corresponds to the *syn* form of the bare molecule and the long-wave band characterized by the long-decaying component of about 1.4 ns seems to be related to the photoproduct of the ESDPT reaction in the doubly hydrogen-bonded dimer (Scheme 3). According to DFT calculations, the position of the absorption maximum of the dimer of the *syn* forms of **PPP**, similarly to the cyclic hydrogen-bonded complexes with methanol, should be shifted to the red by about 1500 cm^{-1} with respect to that of the *syn* form of the molecule. The formation of ground-state dimers, however, is not observed in the absorption spectra; the absorption spectrum of **PPP** in HEX (Figure 1) does not reveal any significant changes with the increase of the concentration between 1.2×10^{-5} mol dm^{-3} and 1×10^{-3} mol dm^{-3}. It is most probable that relative to the monomer, the fraction of the dimers of **PPP** is too small to be observed in the absorption spectra, but the high quantum yield of the tautomeric emission leads to the appearance of the long-wave fluorescence band. Noticeably, the shift to lower energies with respect to the absorption spectrum is observed at

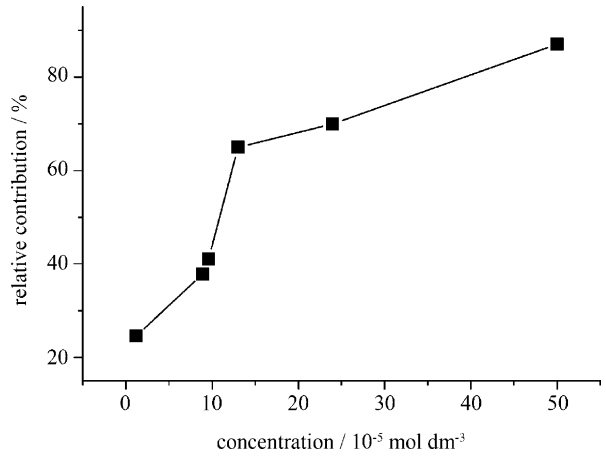

Figure 5. Dependence of the contribution of the 1.4 ns-decay component of the low-energy emission of **PPP** in HEX on the concentration of the solute.

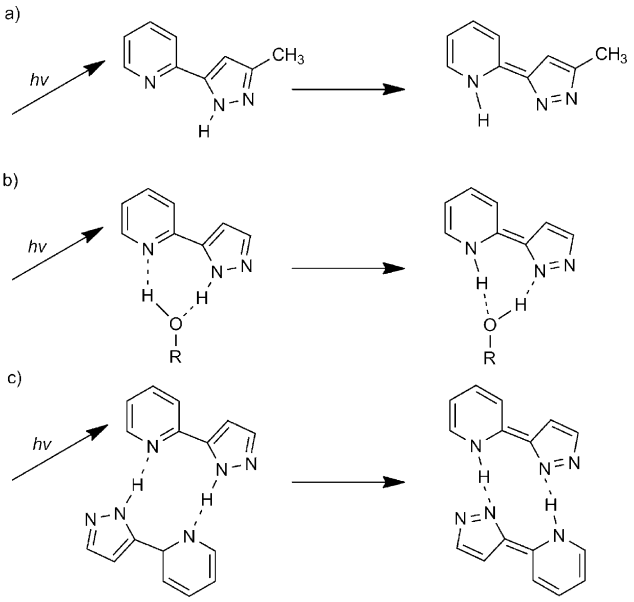

Scheme 3. Scheme of proposed phototautomerization processes for **PPP**, **MPP**, and **BPP**. Excited-state intramolecular proton transfer (ESIPT) in the *syn* rotamer of MPP in HEX (a) and excited-state double proton transfer (ESDPT) in 1:1 complexes of **PPP**, **MPP**, and **BPP** with protic partners (b) and in **PPP** dimer in HEX (c).

the red edge of the excitation spectrum of the long-wave emission (Figure 3). The origin of the long-wave fluorescence characterized by the 380 ps decay is not clear enough. It may be due to the monomeric phototautomer or to the tautomeric form of the complex with residual water.

The dual luminescence of **PPP**, **MPP**, and **BPP** in a mixed solvent containing HEX and 1-PrOH (with the concentration of alcohol varying from $c \cong 1.3\times10^{-2}$–8.8×10^{-2} mol dm^{-3}), can hardly be explained in terms of the bimodal irreversible kinetic model containing only single ground-state species. The data collected in Table 5 corresponds to the highest concentration of alcohol (for this concentration of 1-PrOH the decay curves do not show any components corresponding to the bare molecules). The decay of the short-wave fluorescence of **PPP** (excited at 35700 cm^{-1} and monitored at 30800 cm^{-1}) could be satisfactorily fitted to a three-exponential decay. The best fit involves the decay times of ~21 ps, ~55 ps, and ~213 ps with the relative contributions of ~40%, ~37.5%, and ~22.5%, respectively. On the other hand, the kinetics of the long-wave emission (monitored at 18500 cm^{-1}) is well described by the rise time of 18(±5) ps and the decay time of 630(±50) ps. The ratio of the amplitudes $A_{rise}/A_{decay} = -1.0$ (±0.03) indicates that the long-wave emission is not formed by direct excitation from the ground-state species. The results suggest that of several possible hydrogen-bonded complexes of **PPP** with 1-PrOH, only one undergoes the excited-state proton-transfer reaction. Taking into account the photostationary absorption and fluorescence experiments in the mixed solvents (Figure 4), the long-wave fluorescence can be attributed to the 1:1 cyclic doubly hydrogen-bonded complex between **PPP** and the alcohol partner. Similar results of kinetics investigations were obtained for **MPP** in the mixed solvent. The best three-exponential fit involves the decay times of ~18 ps, ~76 ps, and ~200 ps with the relative contributions of ~22%, ~50%, and ~28%, respectively. In spite of the very low intensity of the low-energy band, the kinetics of the low-energy emission could be satisfactorily fitted to the rise time of 16(±5) ps and the decay time of 280(±30) ps (with contribution of about 94%). The investigations of **BPP** in HEX containing various concentrations of 1-PrOH show even more complex kinetics (the decay of both fluorescence bands is multiexponential, Table 5) than that observed for **PPP** and **MPP**. The kinetic curves corresponding to the low-energy and to the high-energy fluorescence cannot be satisfactorily fitted to a two-exponential model. The three exponential approximation does not improve the fit.

3. Conclusions

The *syn* forms of all the **2-PPs** studied are dominant in nonpolar environments. Increasing the polarity of the solvent leads to a relative stabilization of the *anti1* species (for **PPP**, **MPP**, and **BPP**) and the *anti*, *anti1*, and *syn1* forms (for **NPP**). The short-wave fluorescence of the former three compounds in aprotic solvents originates mainly from the *syn* rotamers.

PPP, **MPP**, and **BPP** emit dual fluorescence in HEX, 1-PrOH, and in aqueous solutions. The low-energy, weak-intensity band, characterized by a huge Stokes shift originates from the product of the excited-state proton-transfer reactions (Scheme 3). This series of compounds is a rare example of molecules that exhibits three types of photoreactions. In agreement with previous investigations,[51] the irreversible ESIPT process takes place in a bare **MPP** in nonpolar environment. Both fluorescence bands are kinetically coupled. The decay of the short-wave fluorescence is recovered in the rise of the low-energy fluorescence. On the other hand, the low-energy emission recorded for **PPP** in HEX is assigned to the phototautomer resulting from the ESDPT reaction in cyclic, doubly hydrogen-bonded dimers, as proved by the effects of the concentration of the solute on the kinetic curves of the low-energy emission. In alcohols and water, all the compounds show an ESDPT process occurring in complexes between the solute molecule and the protic partner. Titration of solutions of **PPP** in HEX with alcohol, in concentrations low enough to prevent the formation of alcohol oligomers, shows that the low-energy fluorescence originates from the complexes of 1:1 stoichiometry. The picosecond kinetics of the phototautomerization process suggests the structure of the complexes. The ESDPT reaction proceeds most probably in cyclic doubly hydrogen-bonded complexes which, under these conditions, are formed in large excess. In bulk alcohol and aqueous solutions, an extremely weak intensity of the low-energy fluorescence results from the existence of different hydrogen-bonded solvates between various forms of the solute and solvent molecules. The majority of these complexes, of various geometries and stoichiometries, are unable to tautomerize.

Acknowledgements

This work was partly supported by grant NN 204 264 238 from the Ministry of Science and Higher Education. The technical assistance of Mrs. Anna Zielińska is greatly appreciated. Time-resolved fluorescence studies were performed in the Centre for Ultrafast Laser Spectroscopy of A. Mickiewicz University in Poznań. We acknowledge the computing grant G17-14 from the Interdisciplinary Centre for Mathematical and Computational Modeling of the Warsaw University.

Keywords: fluorescence · hydrogen bonds · kinetics · photochemistry · proton transfer

[1] R. P. Bell, *The Proton Transfer in Chemistry*, Chapman & Hall, London, **1973**.
[2] R. P. Bell, *The Tunnel Effect in Chemistry*, Chapman & Hall, London, **1980**.
[3] L. G. Arnaut, S. J. Formosinho, *J. Photochem. Photobiol. A* **1993**, *75*, 1.
[4] S. M. Ormson, R. G. Brown, *Prog. React. Kinet.* **1994**, *19*, 45.
[5] D. Le Gourrierec, S. M. Ormson, R. G. Brown, *Prog. React. Kinet.* **1994**, *19*, 211.
[6] J. Catalán, J. C. del Valle, M. Kasha, *Proc. Natl. Acad. Sci. USA* **1999**, *96*, 8338.
[7] J. Waluk, *Conformational Aspects of Intra- and Intermolecular Excited State Proton Transfer in: Conformational Analysis of Molecules in Excited States, Methods in Stereochemical Analysis Series* (Ed.: J. Waluk), Wiley-VCH, Weinheim, **2000**, chap. 2, pp. 57–111, and references therein.
[8] J. Waluk, *Acc. Chem. Res.* **2003**, *36*, 832.
[9] J. Waluk, *Acc. Chem. Res.* **2006**, *39*, 945.
[10] H. Sekiya, K. Sakota, *J. Photochem. Photobiol. C* **2008**, *9*, 81.

[11] A. Mühlpfordt, U. Even, N. P. Ernsting, *Chem. Phys. Lett.* **1996**, *263*, 178.
[12] L. A. Heimbrook, J. E. Kenny, B. F. Kohler, B. W. Scott, *J. Chem. Phys.* **1981**, *75*, 5201.
[13] L. A. Heimbrook, J. E. Kenny, B. F. Kohler, B. W. Scott, *J. Phys. Chem.* **1983**, *87*, 280.
[14] P. M. Felker, W. R. Lambert, A. H. Zewail, *J. Chem. Phys.* **1982**, *77*, 1603.
[15] J. L. Herek, S. Pedersen, S. Bañares, A. H. Zewail, *J. Chem. Phys.* **1992**, *97*, 9046.
[16] A. Douhal, F. Lahmani, A. H. Zewail, *Chem. Phys.* **1996**, *207*, 477.
[17] P. B. Bisht, H. Petek, K. Yoshihara, U. Nagashima, *J. Chem. Phys.* **1995**, *103*, 5290.
[18] F. Lahmani, A. Zehnacker-Rentien, *J. Phys. Chem. A* **1997**, *101*, 6141.
[19] T. Nishiya, S. Yamauchi, N. Hirota, M. Baba, L. Hanazaki, *J. Phys. Chem.* **1986**, *90*, 5730.
[20] C. Su, J. Y. Lin, R. M. R. Hsieh, P. Y. Cheng, *J. Phys. Chem. A* **2002**, *106*, 11997.
[21] M. Kijak, Y. Nosenko, A. Singh, R. P. Thummel, J. Waluk, *J. Am. Chem. Soc.* **2007**, *129*, 2738.
[22] C. A. Taylor, M. A. El-Bayoumi, M. Kasha, *Proc. Natl. Acad. Sci. USA* **1969**, *63*, 253.
[23] K. C. Ingham, M. Abu-Elgheit, M. A. El-Bayoumi, *J. Am. Chem. Soc.* **1971**, *93*, 5023.
[24] K. C. Ingham, M. A. El-Bayoumi, *J. Am. Chem. Soc.* **1974**, *96*, 1674.
[25] P. Avouris, L. L. Yang, M. A. El-Bayoumi, *Photochem. Photobiol.* **1976**, *24*, 211.
[26] C. Chang, N. Shabestary, M. A. El-Bayoumi, *Chem. Phys. Lett.* **1980**, *75*, 107.
[27] J. Waluk, S. J. Komorowski, J. Herbich, *J. Phys. Chem.* **1986**, *90*, 3868.
[28] J. Waluk, J. Herbich, D. Oelkrug, S. Uhl, *J. Phys. Chem.* **1986**, *90*, 3866.
[29] J. Herbich, C.-Y. Hung, R. P. Thummel, J. Waluk, *J. Am. Chem. Soc.* **1996**, *118*, 3508.
[30] Y. Nosenko, G. Wiosna-Sałyga, M. Kunitski, I. Petkowa, A. Singh, W. J. Buma, R. P. Thummel, B. Brutschy, J. Waluk, *Angew. Chem.* **2008**, *120*, 6126; *Angew. Chem. Int. Ed.* **2008**, *47*, 6037.
[31] G. Wiosna-Sałyga, Y. Nosenko, M. Kijak, R. P. Thummel, B. Brutschy, J. Waluk, *J. Phys. Chem. A* **2010**, *114*, 3270.
[32] J. Herbich, J. Dobkowski, R. P. Thummel, V. Hedge, J. Waluk, *J. Phys. Chem. A* **1997**, *101*, 5839.
[33] J. C. del Valle, E. Dominguez, M. Kasha, *J. Phys. Chem. A* **1999**, *103*, 2467.
[34] A. Kyrychenko, J. Herbich, M. Izydorzak, F. Wu, R. P. Thummel, J. Waluk, *J. Am. Chem. Soc.* **1999**, *121*, 11179.
[35] A. Kyrychenko, J. Herbich, F. Wu, R. P. Thummel, J. Waluk, *J. Am. Chem. Soc.* **2000**, *122*, 2818.
[36] D. Marks, H. Zhang, P. Borowicz, J. Waluk, M. Glasbeek, *J. Phys. Chem. A* **2000**, *104*, 7167.
[37] M. Kijak, A. Zielińska, R. P. Thummel, J. Herbich, J. Waluk, *Chem. Phys. Lett.* **2002**, *366*, 329.
[38] Y. Nosenko, M. Kunitski, R. P. Thummel, A. Kyrychenko, J. Herbich, J. Waluk, C. Riehn, B. Brutschy, *J. Am. Chem. Soc.* **2006**, *128*, 10000.
[39] Y. Nosenko, A. Kyrychenko, R. P. Thummel, J. Waluk, B. Brutschy, J. Herbich, *Phys. Chem. Chem. Phys.* **2007**, *9*, 3276.
[40] Y. Nosenko, M. Kunitski, C. Riehn, R. P. Thummel, A. Kyrychenko, J. Herbich, J. Waluk, B. Brutschy, *J. Phys. Chem. A* **2008**, *112*, 1150.
[41] M. Kijak, A. Zielińska, C. Chamchoumis, J. Herbich, R. P. Thummel, J. Waluk, *Chem. Phys. Lett.* **2004**, *400*, 279.
[42] M. Kasha, P. Horowitz, M. A. El-Bayoumi, *Molecular Spectroscopy: Modern Research*, Academic Press, New York, **1972**, p. 287.
[43] M. F. Goodman, *Nature* **1995**, *378*, 237.
[44] A. Douhal, S. K. Kim, A. H. Zewail, *Nature* **1995**, *378*, 260.
[45] D. E. Folmer, L. Poth, E. S. Wisniewski, A. W. Castleman, Jr., *Chem. Phys. Lett.* **1998**, *287*, 1.
[46] J. Catalán, J. C. del Valle, M. Kasha, *Chem. Phys. Lett.* **2000**, *318*, 629.
[47] D. E. Folmer, E. S. Wisniewski, A. W. Castleman, Jr., *Chem. Phys. Lett.* **2000**, *318*, 637.
[48] M. Kijak, I. Petkova, M. Toczek, G. Wiosna-Sałyga, A. Zielińska, J. Herbich, R. P. Thummel, J. Waluk, *Acta Phys. Pol. A* **2007**, *112*, S105.
[49] S. J. Schmidtke, L. A. MacManus-Spencer, J. L. Klappa, T. A. Mobley, K. McNeill, D. A. Blank, *Phys. Chem. Chem. Phys.* **2004**, *6*, 3938.
[50] L. A. MacManus-Spencer, S. J. Schmidtke, D. A. Blank, K. McNeill, *Phys. Chem. Chem. Phys.* **2004**, *6*, 3948.
[51] W.-S. Yu, C.-C. Cheng, Y.-M. Cheng, P.-C. Wu, Y.-H. Song, Y. Chi, P.-T. Chou, *J. Am. Chem. Soc.* **2003**, *125*, 10800.
[52] W. R. Thiel, J. Eppinger, *Chem. Eur. J.* **1997**, *3*, 696.
[53] H. Brunner, T. Scheck, *Chem. Ber.* **1992**, *125*, 701.
[54] M. Ferles, S. Kafka, A. Silhankova, M. Sputova, *Collect. Czech. Chem. Commun.* **1981**, *46*, 1167.
[55] M. A. Khan, A. A. A. Pinto, *J. Heterocycl. Chem.* **1981**, *18*, 9.
[56] J. Jasny, *J. Lumin.* **1978**, *17*, 149.
[57] R. A. Velapoldi, *Considerations on Organic Compounds in Solution and Inorganic Ions in Glasses as Fluorescent Standard Reference Materials* in Proc. Conf. NBS, National Bureau of Standards, Gaithersburg, MD, **1972**, p. 231.
[58] I. Szydłowska, A. Kyrychenko, J. Nowacki, J. Herbich, *Phys. Chem. Chem. Phys.* **2003**, *5*, 1032.
[59] J. Karolczak, D. Komar, J. Kubicki, T. Wróżowa, K. Dobek, B. Ciesielska, A. Maciejewski, *Chem. Phys. Lett.* **2001**, *344*, 154 – 164.
[60] Gaussian 03 (Revision B.03), M. J. Frisch, G. W. Trucks, H. B. Schlegel, G. E. Scuseria, M. A. Robb, J. R. Cheeseman, J. J. A. Montgomery, T. Vreven, K. N. Kudin, J. C. Burant, J. M. Millam, S. S. Iyengar, J. Tomasi, V. Barone, B. Mennucci, M. Cossi, G. Scalmani, N. Rega, G. A. Petersson, H. Nakatsuji, M. Hada, M. Ehara, K. Toyota, R. Fukada, J. Hasegawa, M. Ishida, T. Nakajima, Y. Honda, O. Kitao, H. Nakai, M. Klene, X. Li, J. E. Knox, H. P. Hratchian, J. B. Cross, C. Amado, J. Jaramillo, R. Gomperts, R. E. Stratmann, O. Yazyev, A. J. Austin, R. Cammi, C. Pomelli, J. Ochterski, P. Y. Ayala, K. Morokuma, G. A. Voth, P. Salvador, J. J. Donnenberg, V. G. Zakrzewski, S. Dapprich, A. D. Daniels, M. C. Strain, O. Farkas, D. K. Malick, A. D. Rabuck, K. Raghavachari, J. B. Foresman, J. V. Ortiz, Q. Cui, A. G. Baboul, S. Clifford, J. Cioslowski, B. B. Stefanov, G. Liu, A. Liashenko, P. Piskorz, I. Komaromi, R. L. Martin, D. J. Fox, T. Keith, M. A. Al-Laham, C. Y. Peng, A. Nanayakkara, M. Challacombe, P. M. W. Gill, B. Johnson, W. Chen, M. W. Wong, C. Gonzales, J. A. Pople, Gaussian, Inc., Pittsburgh, PA, **2003**.
[61] S. Simon, M. Duran, J. Dannenberg, *J. Chem. Phys.* **1996**, *105*, 11024.
[62] S. Boys, F. Bernardi, *Mol. Phys.* **1970**, *19*, 553.
[63] M. Cossi, V. Barone, R. Cammi, J. Tomassi, *Chem. Phys. Lett.* **1996**, *255*, 327.
[64] J. Tomasi, B. Mennuci, R. Cammi, *Chem. Rev.* **2005**, *105*, 2999.
[65] V. Barone, M. Cossi, J. Tomasi, *J. Chem. Phys.* **1997**, *107*, 3210.
[66] E. Lim, *J. Phys. Chem.* **1986**, *90*, 6770.
[67] T. Förster, *Z. Elektrochem. Angew. Phys. Chem.* **1950**, *54*, 42.
[68] Z. R. Grabowski, A. Grabowska, *Z. Phys. Chem.* **1976**, *101*, 197.
[69] J. B. Birks, *Photophysics of Aromatic Molecules*, Wiley, New York, **1978**.
[70] J. Michl, E. W. Thulstrup, *Spectroscopy with Polarized Light*, Wiley, New York, **1986**.

Received: July 24, 2012
Published online on September 3, 2012

